https://doi.org/10.26434/chemrxiv.7853414.v1

pH Swing Cycle for CO2 Capture Electrochemically Driven through Proton-Coupled Electron Transfer

Preprint submitted on 15.03.2019, 16:50 and posted on 18.03.2019, 12:43 by Michael Aziz, David G. Kwabi

We propose and perform a thermodynamic analysis of the energetic costs of CO_2 separation from flue gas using a pH swing created by electrochemical redox reactions involving proton-coupled electron transfer from molecular species in aqueous electrolyte. Electrochemical reduction of these molecules results in the formation of alkaline solution, into which CO_2 is absorbed; subsequent electrochemical oxidation of the reduced molecules results in the acidification of the solution, triggering the release of pure CO_2 gas. We examined the effect of buffering from the CO_2-carbonate system on the solution pH during this pH swing cycle, and thus on the open-circuit potential of a hypothetical electrochemical cell in a 4-step CO_2 capture-release cycle. The thermodynamic minimum work input varies from 16 to 75 kJ/mol$_{CO2}$ as throughput increases, for both flue gas and direct air capture, with the potential to go substantially lower if CO_2 capture or release is performed simultaneously with electrochemical reduction or oxidation. These values are compared with those for other separation methods. We discuss the properties required of molecules that would be suitable for such a cycle.

FUNDING

Harvard University Climate Change Solutions Fund

EMAIL ADDRESS OF SUBMITTING AUTHOR
maziz@harvard.edu

INSTITUTION
Harvard John A. Paulson School of Engineering and Applied Sciences

COUNTRY
USA

ORCID FOR SUBMITTING AUTHOR
0000-0001-9657-9456

DECLARATION OF CONFLICT OF INTEREST
No conflict of interest

VERSION NOTES
Version 1, Thermodynamic cycle

https://doi.org/10.26434/chemrxiv.7853414.v1

pH Swing Cycle for CO_2 Capture Electrochemically Driven through Proton-Coupled Electron Transfer

David G. Kwabi[†] and Michael J. Aziz*
Harvard John A. Paulson School of Engineering and Applied Sciences
29 Oxford St.
Cambridge MA 02138 USA

*maziz [at] harvard [dot] edu
[†]Present address: Department of Mechanical Engineering, University of Michigan, Ann Arbor MI 48109 USA. dkwabi [at] umich [dot] edu

15 March 2019

Abstract

We propose and perform a thermodynamic analysis of the energetic costs of CO_2 separation from flue gas (0.1 bar CO_2(g)) and air (400 ppm CO_2) using a pH swing created by electrochemical redox reactions involving proton-coupled electron transfer from molecular species in aqueous electrolyte. In this scheme, electrochemical reduction of these molecules results in the formation of alkaline solution, into which CO_2 is absorbed; subsequent electrochemical oxidation of the reduced molecules results in the acidification of the solution, triggering the release of pure CO_2 gas. We examined the effect of buffering from the CO_2-carbonate system on the solution pH during this pH swing cycle, and thus on the open-circuit potential of a hypothetical electrochemical cell in a 4-step CO_2 capture-release cycle. The thermodynamic minimum work input varies from 16 to 75 kJ/mol$_{CO2}$ as throughput increases, for both flue gas and direct air capture, with the potential to go substantially lower if CO_2 capture or release is performed simultaneously with electrochemical reduction or oxidation. These values are compared with those for other electrochemical and thermal CO_2 separation methods. We discuss the properties required of molecules that would be suitable for such a cycle.

Introduction

Accumulating CO_2 emissions from the burning of fossil fuels [1] are resulting in a historically unprecedented rate of climate change. Consequently, there are increasing efforts worldwide to reduce societal reliance on fossil fuel-based energy and to switch to carbon-free sources such as

nuclear, solar, wind and geothermal [2]. According to the Intergovernmental Panel on Climate Change, average atmospheric CO_2 concentrations have to stay below roughly 500 ppm in order to avoid severe consequences of global warming (greater than 2 °C above pre-industrial era levels) and irreversibly deleterious changes to natural habitats and ecosystems that would threaten the viability of human civilization [3]. Given, however, that the global rate of transition to low-carbon sources is presently not nearly fast enough to avoid this threshold, other approaches are urgently required to deal with the problem of rising CO_2 concentrations.

Among the most promising of these is carbon capture and sequestration (CCS), in which CO_2 is separated from a point source [4] (e.g. flue gas from a coal or natural gas power plant), compressed, and sequestered away from the atmosphere. A variant on this idea is direct air capture (DAC) [5], in which CO_2 is captured directly from ambient air, compressed and sequestered. These strategies recognize the continued use of fossil fuels while combating atmospheric CO_2 accumulation. In principle, the pure CO_2 obtained after separation can be converted back into chemical fuels with carbon-free energy, thus providing fuels without added CO_2 emissions; this is an active research area.

CO_2 separation from mixed gases is the most energetically demanding step of CCS, and much effort has gone into developing separation techniques that expend as little energy as possible per unit of CO_2 captured. Most well-developed means for doing so are "temperature-swing" cycles that involve contacting CO_2 with a strongly basic chemical sorbent in an absorption step, and then heating the CO_2-rich sorbent to release pure CO_2. The overall energy input required for temperature-swing cycles, however, is high (> 120 kJ/mol$_{CO2}$) as compared to the minimum thermodynamic free energy requirement for carbon capture from air (20 kJ/mol$_{CO2}$) or flue gas with 0.1 bar CO_2 (6 kJ/mol$_{CO2}$) [6]. It is worth noting that CCS from flue gas with a monoethanolamine (MEA)-based sorbent would require roughly 30% of the heat energy produced by coal-powered plants from combustion to be consumed by carbon capture[4], thereby making it unavailable for electricity production. As a result, other sorbents and strategies are actively being explored both in fundamental research and industry.

The use of hydroxide (OH^-) in alkaline aqueous solutions to capture CO_2, in the reactions $OH^- + CO_2 \rightarrow HCO_3^-$ and, subsequently, $HCO_3^- + OH^- \rightarrow CO_3^{2-} + H_2O$, has received renewed interest in recent years as part of a viable separation approach. DAC using strongly alkaline solution to absorb CO_2 in a high-surface-area contactor, followed by a chemical regeneration cycle that uses thermal energy to subsequently release it from solid carbonate precipitates [7, 8], has begun commercialization. This process has an energetic cost that is comparable to that of many temperature-swing-based processes, but its potentially low financial cost (\$94 - \$232/ton$_{CO2}$) for DAC makes practical application on a wide scale more feasible. [8]

The potential simplicity and low cost of implementation of CCS approaches that use alkaline solutions thus represents a substantial opportunity in emissions mitigation. In this study, we propose an electrochemically mediated CO_2 separation approach that uses a large electrochemically-induced swing in solution pH to absorb and release CO_2 and requires electrical but no thermal energy input. Informed by our previous work on using quinones in organic redox-flow batteries [9], this approach relies on the use of small molecules that undergo proton-coupled electron transfer (PCET) in aqueous solution. Electrochemical reduction/oxidation ("redox") of these molecules results in proton uptake/release, respectively [10, 11], resulting in changes in solution pH [12] which, if large enough, can cause CO_2 to be strongly absorbed at high pH (> 12) and released at low pH (< 5).

In this paper we carry out a thermodynamic analysis of the energetic cost of this electrochemical process and calculate the minimum required electrical energy input per mole of CO_2 for an ideal cycle based on the potential difference between applied reduction and oxidation potentials vs. pH. The results show the minimum work input for this scheme is 16 – 75 kJ/mol$_{CO2,}$ depending on the separation throughput per cycle, for capture from both flue gas and atmosphere. PCET with organic molecules that undergo kinetically rapid redox reactions [9] is potentially a promising electrochemical basis for practicable CCS, as it may both reduce energetic losses and lower overall costs per ton of CO_2 separated, due to the low cost of these chemicals.

Results and Discussion

In order to effect large changes in solution pH using PCET in aqueous media containing CO_2, buffering from inorganic carbon species must be overcome. Thus, we first examine the dependence of pH on the constituents of dissolved inorganic carbon (DIC) species present in solution, namely aqueous CO_2 ($CO_2(aq)$), bicarbonate (HCO_3^-) and carbonate (CO_3^{2-}) [13]:

$$DIC = [CO_2(aq)] + [HCO_3^-] + [CO_3^{2-}]. (1)$$

The relative ratios of these species at equilibrium is dictated by the reactions between aqueous CO_2 and water:

$$CO_2(aq) + H_2O \overset{K_1}{\Leftrightarrow} HCO_3^- + H^+ \overset{K_2}{\Leftrightarrow} CO_3^{2-} + 2H^+$$

where K_1 and K_2 are the first and second dissociation constants of carbonic acid (H_2CO_3), respectively, and defined as the following equilibrium constants:

$$K_1 = \frac{[HCO_3^-][H^+]}{[CO_2(aq)]}; (2)$$

$$K_2 = \frac{[CO_3^{2-}][H^+]}{[HCO_3^-]}. (3)$$

For a solution of zero salinity, K_1 and K_2 are 1.1×10^{-6} M and 4.1×10^{-10} M [14], resulting in the first and second pKa for carbonic acid being 6.0 and 9.4, respectively. Thus, in acidic solutions of pH < 6 total DIC is composed primarily of dissolved $CO_2(aq)$, in basic solutions of pH > 9.4 total DIC is composed primarily of carbonate anions, and for the intermediate pH range total DIC is composed primarily of bicarbonate anions.[13] Because $CO_2(aq)$, being uncharged, is the only form that exchanges with the atmosphere, increasing the pH of a solution drives down the activity of $CO_2(aq)$, leading to net dissolution of $CO_2(g)$ as $CO_2(aq)$. Correspondingly, decreasing the pH raises the activity of $CO_2(aq)$, leading to outgassing. This provides a mechanism for selectively absorbing CO_2 from a mixture of gases, and then releasing a pure stream at a separate point for sequestration. Given that certain bicarbonate/carbonate compounds have exceptionally high solubilities (> 3 M at room temperature) in water, this strategy affords a potential pathway for high-throughput separation of CO_2 from air or flue gas. Additionally, the fact that the entire process

takes place in the liquid phase offers a potentially simpler and lower-cost CCS route as compared to schemes in which, having absorbed CO_2 using alkaline solution, precipitation and heating of solid carbonates is required to release gaseous CO_2.[7, 8, 15]

We envision a thermodynamic cycle comprising a series of alternating electrochemical and gas-liquid exchange processes: (1) electrochemical acidification of an electrolyte at constant DIC concentration, resulting in supersaturation of aqueous CO_2; (2) outgassing of pure CO_2 gas at the collection stream until gas-liquid equilibrium is reached; (3) electrochemical de-acidification of the electrolyte, resulting in strongly alkaline electrolyte; and (4) invasion of CO_2 from air/flue gas into the alkaline electrolyte. During each process, the constituents of DIC and pH can be described based on CO_2-carbonate and water dissociation equilibria, as well as the principle of charge conservation. Based on the definition of DIC set forth in equation 1, the concentration of each component of DIC as a function of total DIC and $[H^+]$ is given by [13]

$$[CO_2(aq)] = \frac{DIC}{1 + \frac{K_1}{[H^+]} + \frac{K_1 K_2}{[H^+]^2}}; \quad (4)$$

$$[HCO_3^-] = \frac{DIC}{1 + \frac{[H^+]}{K_1} + \frac{K_2}{[H^+]}}; \quad (5)$$

$$[CO_3^{2-}] = \frac{DIC}{1 + \frac{[H^+]}{K_2} + \frac{[H^+]^2}{K_1 K_2}}. \quad (6)$$

An additional constraint is given by the water dissociation equilibrium $H_2O \overset{K_w}{\Leftrightarrow} H^+ + OH^-$ resulting in

$$[H^+][OH^-] = 10^{-14}\ M^2. \quad (7)$$

Given the ionic species present, assuming the presence of an electrolyte salt that comprises cationic and anionic species S^+ and S^-, respectively, and imposing a charge neutrality constraint results in:

$$[S^+] - [S^-] = [OH^-] + [HCO_3^-] + 2[CO_3^{2-}] - [H^+]. \quad (8)$$

The total alkalinity (TA) of the solution under consideration is defined as [13]

$$TA \equiv [OH^-] + [HCO_3^-] + 2[CO_3^{2-}] - [H^+]. \quad (9)$$

153 which is numerically equal to the difference between S^+ and S^- concentrations according to Eq. (8).
154 It is important to note that PCET, involving the transfer of protons between a small molecule Q
155 and solution, may directly change the solution TA. To understand this, consider the case of an
156 electrochemical reduction reaction such as $Q + e^- + xH^+ \leftrightarrow QH_x{}^{x-1}$ where x is the number of
157 protons transferred per electron. To the extent that the satisfaction of charge neutrality following
158 the reduction of Q is not fully accounted for by a change in DIC, $[H^+]$ or $[OH^-]$ content of the
159 solution, it would result in a net increase in TA – i.e. either *via* a transfer of S^- out of the solution
160 or a transfer of S^+ into it. Likewise, oxidation of $QH_x{}^{x-1}$ might yield a net decrease in TA. Changes
161 in TA cause changes in pH; we stress, however, that TA and pH are not linearly related to each
162 other: electrochemically induced perturbations to TA affect pH only subject to equilibria
163 represented by equations 4 – 9 being satisfied. In other words, PCET provides a driving force for
164 pH swing through changing TA, but *actual* changes in pH depend on buffering from the CO_2-
165 carbonate equilibrium.
166
167 We determine the minimum work required to separate CO_2 from a mixed gas stream using an
168 electrically-driven pH-swing cycle involving these chemical and electrochemical processes. The
169 four processes described above are represented schematically in **Figure 1**, in which process 1→ 2
170 and 3 → 4 are constant DIC, electrochemical processes – associated with electrical energy
171 input/output - whereas processes 2 → 3 and 4 → 1 involve gas-liquid exchange of CO_2 at open
172 circuit potential and constant TA. All processes are assumed to be isothermal.

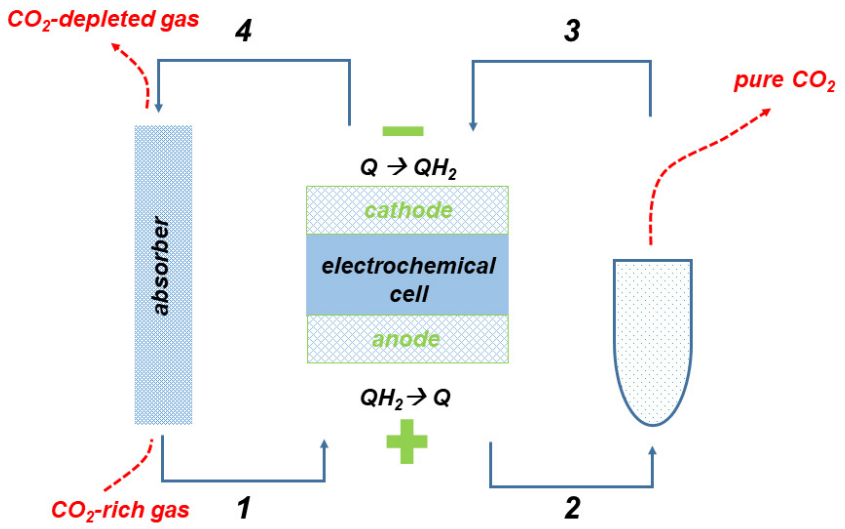

Figure 1. Schematic of electrochemical CO_2 separation cycle, showing flow of liquid electrolyte (in blue lines) and gas (dashed red lines) between the electrochemical cell and gas-liquid exchange chambers, with various states numbered. Processes between numbered states are: electrochemical acidification (1 → 2), CO_2 outgassing (2 → 3), electrochemical de-acidification (3 → 4) and CO_2 invasion (4 → 1).

We first perform a preliminary calculation to determine the equilibrium TA at State 1, i.e. after CO_2 invasion and before electrochemical acidification, for given values of DIC and CO_2 partial pressure. **Figure 2** shows the result of this analysis, in which solutions were found to the system of equations 4 – 8 for two initial CO_2 partial pressures: 0.1 bar and 400 ppm CO_2(g), which correspond to the CO_2 concentration of flue gas from a typical coal power plant and atmospheric CO_2, respectively. [CO_2(aq)] is assumed to be fixed based on a Henry's Law constant of 35 mM/bar at room temperature. The results show that for both conditions, TA has an almost linear relationship to DIC, with $DIC = 0.86 \times TA$ at 0.1 bar CO_2(g), and $0.53 \times TA$ at 400 ppm CO_2(g). Solution pH also increases with DIC, settling close to 8.6 in the limit of high DIC at 0.1 bar CO_2(g) (**Figure 2**a) and 9.8 at 400 ppm CO_2 (**Figure 2**b). An important reference point for these results is seawater in equilibrium with atmospheric CO_2, which mainly comprises HCO_3^- and is known to have a natural pH of about 8.1 for a DIC of ~ 2 mM [13]. Results in **Figure 2**b are consistent with this expectation, as at a DIC of 2 mM the solution pH is 8.1.

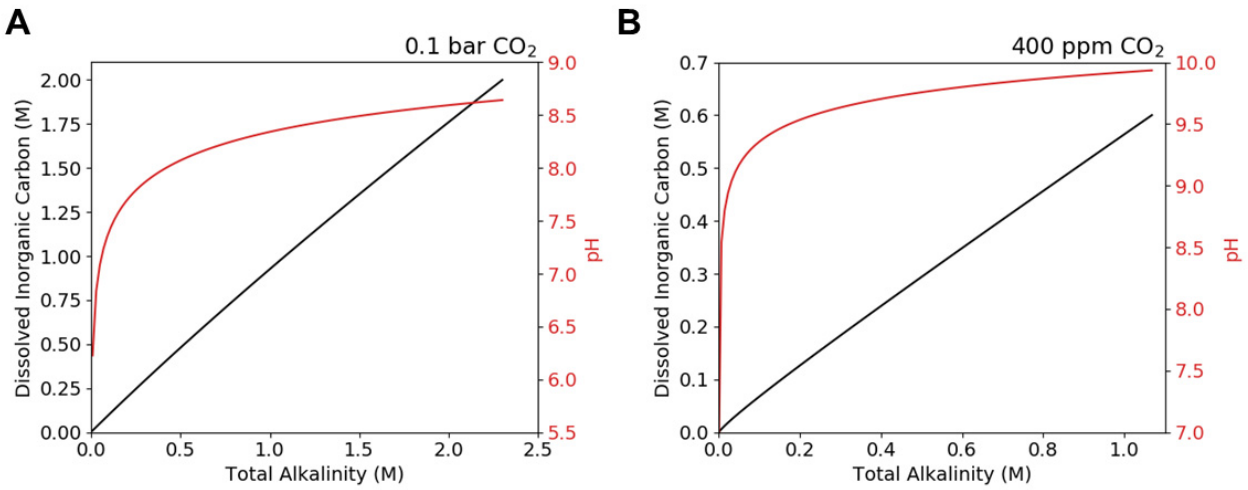

Figure 2. DIC (black) and pH (red) as functions of TA at CO_2 partial pressures of (a) 0.1 bar and (b) 400 ppm.

We next consider the minimum concentration of PCET-active molecules required for process 1→2 i.e. electrochemical acidification of the electrolyte at a fixed DIC. **Figure 3** shows the minimum concentration of a hypothetical small molecule capable of concerted $2H^+$, $2e^-$ PCET that is required to convert all DIC to CO_2(aq). CO_2 concentrations at the CO_2-rich gas inlet of 0.1 bar and 400 ppm were considered, and the TA at State 1 was calculated based on the relationship between DIC and TA shown in **Figure 2**. Conversion of all carbonate/bicarbonate was deemed complete at the point where 99% of DIC is composed of CO_2(aq), after electrochemical acidification *via* QH_2 oxidation. For both inlet conditions, a linear relationship between DIC and minimum concentration of QH_2, or $[QH_2]_{min}$, was obtained, with $[QH_2]_{min}$ equal to $0.57 \times DIC$ for the inlet with 0.1 bar CO_2, and $0.93 \times DIC$ for that with 400 ppm CO_2, for DIC values in the range between 0 and 2.5 M.

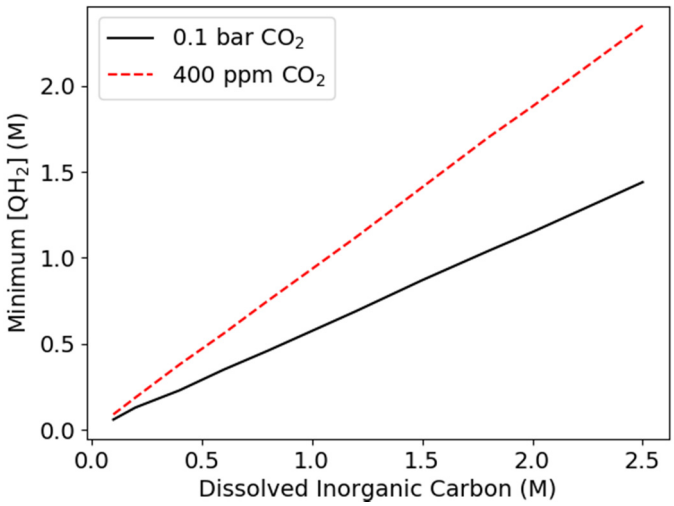

Figure 3. Minimum concentration of QH_2 required to convert 99% of all DIC to CO_2(aq).

We now calculate the minimum work input required to separate CO_2 in the ideal cycle defined above. As an example of a desirable implementation, we assume an inlet CO_2 partial pressure of 0.1 bar and a starting [QH_2] of 1.4 M, which translates to a maximum convertible DIC of 2.46 M. The minimum work input is sensitive to two important parameters: the ratio of partial pressures of CO_2 at the exit to inlet stream, which we term the 'exit/inlet pressure ratio', and the CO_2 supersaturation at State 2, the start of outgassing. We define CO_2 supersaturation here as the ratio of [CO_2(aq)] at the start of outgassing compared to equilibrium value of [CO_2(aq)] at the exit. As the exit/inlet pressure ratio increases, the work of separation increases. CO_2 supersaturation at State 2, which we denote hereafter as 'outgassing overpressure', is proportional to CO_2 separation throughput as, for a given exit/inlet pressure ratio, it is a measure of how much dissolved CO_2 can be released in a single cycle. For the implementation under consideration, an exit/inlet pressure ratio of 10 was assumed (i.e. 1 bar of pure CO_2(g) at the exit stream, for 0.1 bar inlet partial pressure), resulting in an outgassing overpressure of 69. **Figure 4**a shows the pH of the solution as a function of *Q* concentration during electrochemical acidification, going from initial pH of 8.7 to 4.3 when complete conversion is achieved.

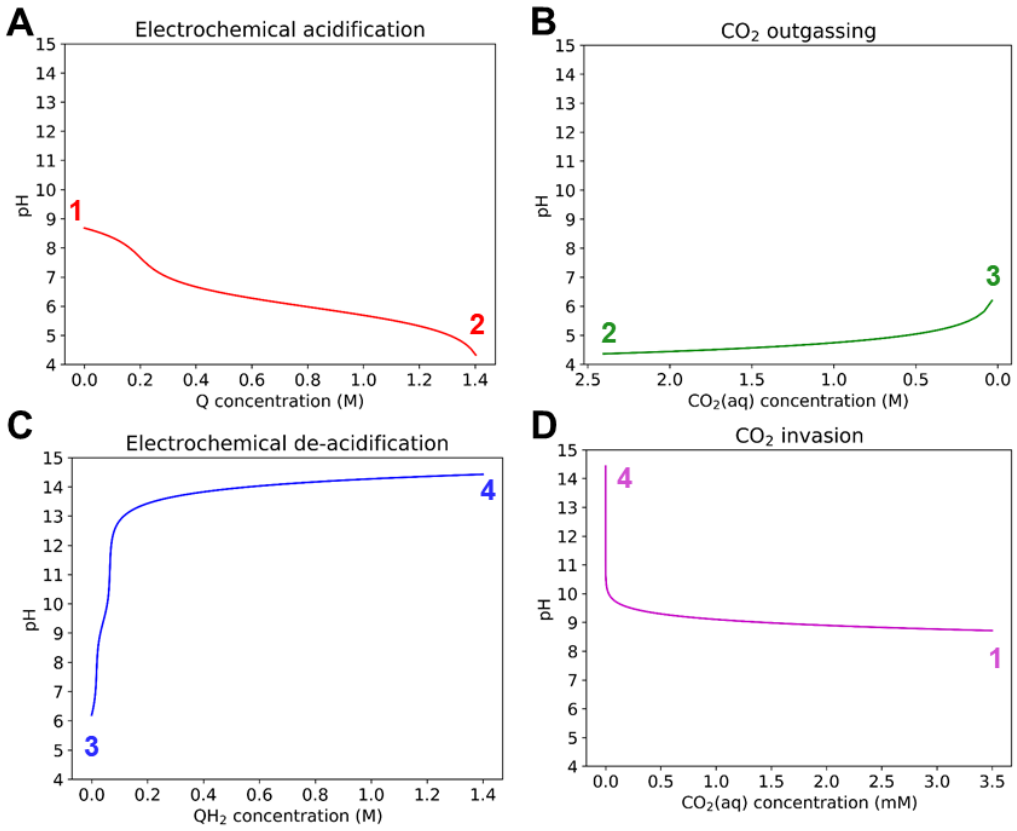

Figure 4. pH as a function of Q, QH_2, and CO_2(aq) concentrations for an ideal CO_2 separation cycle with inlet and outlet CO_2(g) of 0.1 and 1 bar, respectively, during (a) electrochemical acidification (process 1 → 2, in red) (b) CO_2 outgassing at 1 bar CO_2(g) (process 2→ 3, in green) (c) electrochemical de-acidification (process 3 → 4, in blue) and (d) CO_2 invasion (process 4 → 1, in magenta), at the end of which aqueous CO_2 (CO_2(aq)) is assumed to be in equilibrium with 0.1 bar CO_2 gas. A starting value of [QH_2] of 1.4 M and a DIC value at State 1 of 2.46 M are assumed.

For the outgassing process 2→3 (**Figure 4**a), equations 4 - 8 are solved subject to the constraint that TA is fixed and, that at the end of the process, [CO_2(aq)] relaxes to its equilibrium value at 1 bar of 35 mM. After this, process 3→ 4 (electrochemical de-acidification) is evaluated with DIC fixed at its value at State 3, using parameters from State 3 as inputs (**Figure 4**c); the pH goes from 6 to ~14.5 as the concentration of QH_2 increases. CO_2 invasion (**Figure 4**d) then occurs, completing the cycle and restoring State 1. The relationship between DIC and pH throughout the cycle is shown in **Figure 5**, whereas that between pH and [CO_2(aq)] is shown in **Figure S1**. For comparison, an ideal cycle assuming a more moderate reactant solubility (i.e. the lower of Q and

QH_2 solubilities) of 0.1 M (resulting in DIC at State 1 of 0.175 M) is shown in Figure S2. An important consequence of the lower solubility is that the pH after electrochemical de-acidification (process 3 → 4) is 13, rather than 14.5; this is a direct result of the lesser degree of de-acidification afforded by the removal of 0.2 M H^+ from solution, as opposed to 2.8 M H^+ (i.e. assuming $2H^+$,2e- redox processes in both the 0.1 M and 1.4 M solubility cases). As will be discussed presently, the pH attained after process 3 → 4 is an important metric that constrains the selection of viable molecules for electrochemical CCS. It is also important to note that based on the relationship between DIC value and minimum [QH_2] required for full acidification shown in **Figure 3**, the concentration of QH_2 at State 1 constrains combinations of exit/inlet pressure ratio and outgassing overpressure that may be used in an ideal cycle. An illustration of this is given in Figure S3, which shows lines of constant [QH_2] for different exit/inlet pressure ratios and outgassing overpressures. As expected, higher outgassing overpressures and exit/inlet pressure ratios require higher concentrations of starting [QH_2] to run a cycle.

In calculating the energetic cost/mol CO_2 separated, we note that only processes 1→ 2 and 3 → 4 involve work inputs/outputs to or from the electrochemical cell, respectively. Using the Nernst equation and assuming dilute solutions, we relate the pH during each of those processes to the redox potential (E_R) of the electrode at which conversion between the pairs of the *Q/QH₂* redox couple occurs: $E_R = E_0 - (59mV \times pH)$ where E_0 is the redox potential under standard conditions, in which pH = 0.

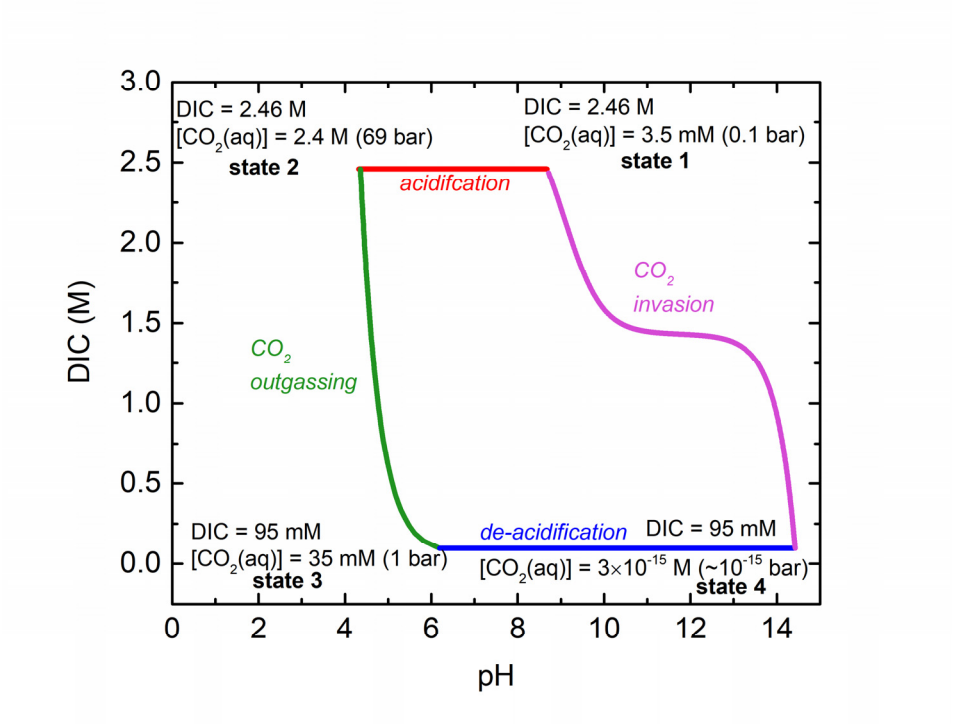

Figure 5. DIC vs. pH during the 4-process cycle described in **Figure 4**. At each numbered state, DIC, [CO_2(aq)], and equilibrium CO_2(g) corresponding to the value of [CO_2(aq)] are reported.

Figure 6 shows the result of this calculation for electrochemical acidification and de-acidification, where the area between the potential profiles represents the net electrical energy input. Dividing this area by the absolute difference in [CO_2(aq)] between states 2 and 3 yields the overall work input per mole of CO_2 captured, $\overline{w}$, which may be represented as follows:

$$\overline{w} = \frac{2F}{\Delta c_{CO2(aq)}} \oint E \, dq$$

Here, F is Faraday's constant of 96,485 C/mol, $\Delta c_{CO2(aq)}$ represents the difference in aqueous CO_2 concentration before and after CO_2 outgassing, E is redox potential, and the factor of 2 results from the assumption that each Q/QH_2 species undergoes a 2-electron redox process. In the implementation under consideration, the net electrical energy input is 50 kJ/mol$_{CO2}$.

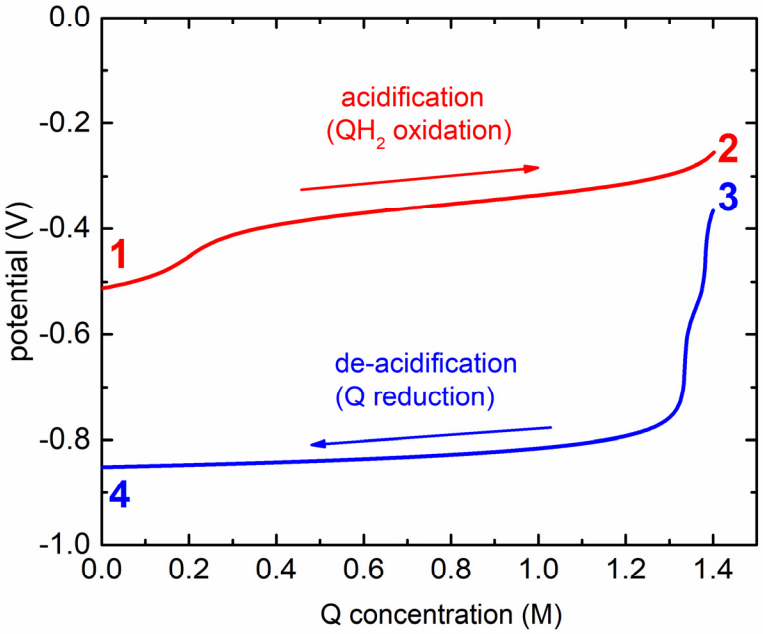

277

278 **Figure 6**. Redox potential as a function of Q concentration during electrochemical acidification
279 (red line, process 1→ 2) and de-acidification (blue line, process 3 → 4) for ideal CO_2 separation
280 cycle of **Figure 5**.

281

282 Following a program similar to that sketched out above, **Figure 7** shows the ideal cycle work input
283 required for CO_2 separation from inlet streams with 0.1 bar CO_2 (**Figure 7**a) and 400 ppm CO_2
284 (**Figure 7**b), for exit/inlet pressure ratios that result in CO_2 release around 1 bar at a variety of
285 outgassing overpressures. Ideal cycle work is compared to the thermodynamic minimum work of
286 separation required to provide the increase in CO_2 exergy, which, is directly related to the partial
287 pressures of CO_2 at the inlet and exit streams[4, 6]: $RT\ ln\frac{P_3}{P_1}$, where R is the molar gas constant of
288 8.314 J/mol K and temperature T is assumed to be 293.15 K (20 °C). For a given exit/inlet pressure
289 ratio, the ideal cycle work input increases with outgassing overpressure, up to ~ 50 and
290 75 kJ/mol$_{CO2}$ for outgassing overpressures of 100 for inlets of 0.1 bar and 400 ppm CO_2(g),
291 respectively. This is expected as a consequence of the fact that increasingly higher CO_2 super-
292 /undersaturation during the outgassing and invasion processes, respectively, causes increasingly
293 greater exergetic losses; these losses contribute to the difference in average pH, and thus redox
294 potential, of the electrolyte during electrochemical acidification and de-acidification (**Figure 6**).

In order to reduce exergetic losses – and thus the ideal cycle work input - one might consider performing CO_2 invasion and outgassing simultaneously with electrochemical acidification and de-acidification, respectively; this way, extremes in solution pH, and potential, are avoided. Exemplary applications of this strategy during electrochemical de-acidification and acidification are presented in Figure S4 where, for the cycle outlined in **Figure 4**, processes 1 → 2 and 2 → 3 are combined into one two-part process: electrochemical acidification at constant DIC until [CO_2(aq)] reaches its equilibrium value at 1 bar CO_2(g) of 35 mM, followed by outgassing at constant [CO_2(aq)] until [Q] reaches 1.4 M. This results in a decrease in the ideal cycle work input from 50 to 42 kJ/mol$_{CO2}$. A similar approach can be applied to processes 3 → 4 and 4 → 1, with electrochemical de-acidification at constant DIC until [CO_2(aq)] is 3.5 mM, followed by CO_2 invasion at constant [CO_2(aq)] until [QH_2] reaches 1.4 M. As large exergetic losses during CO_2 invasion are avoided, this results in a reduction in the ideal cycle work from 50 kJ/mol$_{CO2}$ to 14 kJ/mol$_{CO2}$. Combining both strategies in one two-process cycle that features zero exergetic losses results in an ideal cycle work input of 5.7 kJ/mol$_{CO2}$, which is equal to the thermodynamic minimum work input. In practice, however, this strategy may come at the cost of lower CO_2 separation throughput, as CO_2 outgassing/invasion kinetics increase with lower/higher pH's, respectively.[16] The use of homogeneous catalysts such as carbonic anhydrase [17-19] to speed up CO_2 invasion/outgassing kinetics may be one way of making such a cycle practical.

It is worth noting that CO_2 separation can, in principle, be run at arbitrarily high exit/inlet pressure ratios, and thus higher exit stream CO_2 partial pressures than indicated in **Figure 7**. However, as already illustrated in Figure S3, one would need increasingly higher concentrations of the PCET-active molecule, the solubility of which is constrained in reality (discussed in more detail below). Figure S5 illustrates such a high-pressure exit stream case, where ideal cycle work is plotted vs a series of exit/inlet pressure ratios, the highest of which yield CO_2 separation from either 0.1 bar or 400 ppm to 150 bar i.e. approaching typical CO_2 pipeline pressures. Assuming an upper limit in QH_2 solubility of 10 M, our model predicts maximum achievable outgassing overpressures of approximately 3 and 2 for flue gas (Figure S5a) and DAC (Figure S5b), at work inputs of 40 and 70 kJ/mol$_{CO2}$, respectively.

Several factors dictate the practical feasibility and optimal operation of an electrochemical CO_2 separation cycle based on the above scheme. With regard to a chosen redox pair Q/QH_2, high chemical stability in aqueous solution and fast redox kinetics are desirable for stable long-term operation and low activation losses. And, especially for CCS schemes in which oxygen composes a large fraction of the inlet gas composition (as in DAC), a high redox potential would be necessary to reduce or even eliminate the thermodynamic susceptibility of QH_2 to reversible chemical oxidation by O_2, which would cause an efficiency loss and possibly a cell electrolyte imbalance as well.

The most important attribute of Q, however, has to do with the highest pH it can effect upon being reduced during electrochemical de-acidification, as this determines the maximum value of DIC that can be deployed in a full CCS cycle and thus, the maximum CO_2 separation throughput per cycle. Higher values of DIC entail higher outgassing overpressures, which will require higher pH values to be achieved after electrochemical de-acidification (a final pH of 14.5 is required for an overpressure of 69 where DIC is 2.46 M, and a pH of 13 for an overpressure of 5 where DIC is 0.175 M, as shown in **Figure 4**c and Figure S2c, respectively). In the ideal cycle under consideration, the hypothetical redox pair is considered capable of concerted $2H^+$, $2e^-$ PCET at all pH values, however in real aqueous solutions, PCET would be strongly affected by the affinity of the reduced reactant for protons. A common measure of this proton affinity is the pK_a of the protonated form of the reduced reactant, which is calculated based on the equilibrium between its protonated and deprotonated variants. A simplified reaction equation representing this equilibrium is:

$$QH_2 \leftrightarrow Q^{2-} + 2H^+$$

Here, the equilibrium constant for this reaction is $K_a = \frac{[Q^{2-}][H^+]^2}{[QH_2]}$; and the pKa is defined as the logarithmic constant, $-\log_{10} K_a$. As this equilibrium is highly sensitive to solution acidity, increasingly basic solutions will favor the formation of the deprotonated Q^{2-} rather than QH_2, in which case reduction of Q will not result in solution de-acidification as assumed. Based on the pK_a values and the water dissociation equilibrium, as well as the conservation of the total concentration of the molecule in all redox states, the ideal relationship between pK_a, Q concentration (i.e. concentration of the oxidized form of the molecule) and final pH was derived, and is depicted in Figure S6 (see calculations in SI). As expected, the final pH scales strongly with pK_a, but is limited

at low Q/QH_2 solubilities. As an illustration, consider a solution of Q with pK_a 15 – at a concentration of 50 mM, it will reach only pH 13 (equivalent to 100 mM OH^-) upon bulk electrolytic reduction, but will achieve a pH of 14.7 for a Q concentration of 4.0 M. Finding redox-active species with a combination of high solubility and high pKa is therefore critical for reaching high DIC values in the electrochemical cycle, and thereby enabling high-throughput CO_2 separation.

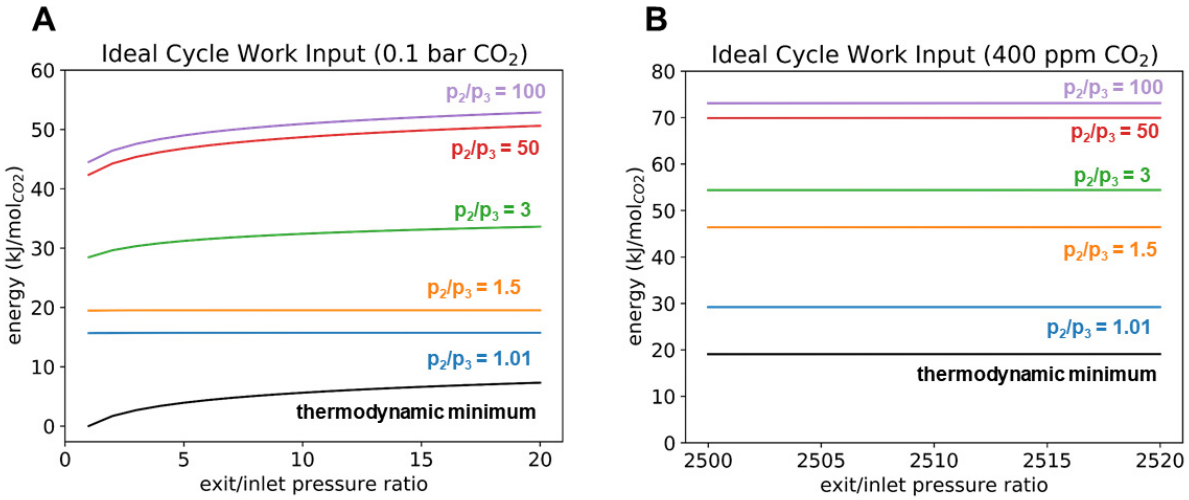

Figure 7. Ideal cycle work as a function of the exit/inlet pressure ratio, p_3/p_1, for various values of the outgassing overpressure, p_2/p_3, for inlet streams of (a) 0.1 bar CO_2 and (b) 400 ppm CO_2. Exit/inlet pressure ratios around 2500 are plotted as this is relevant to DAC, where CO_2 is separated from 400 ppm to 1 bar. Both measures are compared against the minimum work of separation at each exit/inlet pressure ratio.

Although DIC values greater than 3 M can, in principle, be attained in aqueous solution (room-temperature solubilities for $NaHCO_3$, Na_2CO_3, $KHCO_3$ and K_2CO_3 are 11.4, 3.2, 3.3 and 8.1 M, respectively), solubilities of molecules capable of undergoing PCET across a wide pH range are typically lower, and thus limit DIC values that can be utilized in an electrochemical CCS cycle.

There has been extensive research into organic molecules capable of PCET, in part because it is pivotal in many biological energy-conversion processes such as respiration and photosynthesis.[20] In the field of aqueous organic redox-flow batteries (RFBs) in particular, it

has been shown that several quinone-based molecules can undergo $2H^+$, $2e^-$ PCET with fast kinetics. One major drawback, however, is that these molecules typically have pK_a's that are < 11.0, and solubilities < 1.0 M.[21-24] 1,2-benzoquinone-3,5-disulfonic acid is a rare exception in the latter category, with a reported solubility of 3.0 M, however its chemical instability in water [25] renders it unattractive for electrochemical CO_2 separation. Aza-aromatic redox-active compounds [22] are potentially more promising in terms of both high solubility and pK_a. Although it does not participate in PCET for most of the 0 – 14 pH range, quinoxaline has been shown to have a solubility above 4.0 M in water and in weakly alkaline aqueous solution.[26] Phenazine, however, participates in $2H^+$, $2e^-$ PCET up to at least pH 13 [27]. To our knowledge, among organic molecules that can undergo PCET for RFBs, phenazine dihydroxysulfonic acid has the highest solubility yet reported (1.8 M), and it is reasonably chemically stable (i.e. decomposing at < 1 %/day).[28] Besides organic molecules, polyoxometalates have attracted interest as potentially highly soluble candidates for reactants in RFBs[29, 30] and redox mediators for water splitting/reduction [30, 31]. Although they tend to be insoluble and redox-inactive in basic solution [32], they are, in principle, capable of greater than 2 H^+, $2e^-$ PCET. Chen *et al.*[30] have demonstrated that a tungsten-based polyoxoanion can stably undergo an 18 H^+, 18 e^- redox process at a concentration of 0.5 M, with the potential to go up to 2.0 M, although its behavior in basic solution was not reported. The development of a similar reactant capable of PCET across the pH 3 - 13 range would effect a much larger pH swing per mole of reactant than heretofore assumed, thus lowering the required reactant solubility. Indeed, continued exploration of the large parameter space to which inorganic and organic redox-active species belong may yield candidates for electrochemical CO_2 separation that boast higher solubility and pK_a than those assumed here, and applying insights from the fields of electrocatalysis and energy storage may prove beneficial toward that goal.

Another critical question bearing on the practical implementation of this scheme relates to the nature of the electrochemical cell, and how it is integrated with CO_2 capture and release. In **Figure 1** it is assumed that these processes occur in steady-state: the electrolyte flows between an air contactor [15, 33] at the inlet, where CO_2 absorption occurs at high pH; an electrochemical cell where acidification/de-acidification take place; and the exit, where CO_2 is released at low pH. In order to maintain this pH gradient across the electrodes of the cell, it would be critical to have an

ion-selective membrane that would strongly suppress the permeation of any ions that affect the solution TA (i.e. ions on the right hand side of equation 9). An anion-exchange membrane (AEM) with high perm-selectivity for Cl^- ions would be particularly ideal for this purpose, but a high concentration of Cl^- would be needed in practice to limit the amount of crossover of hydroxide, which has a higher mobility than Cl^-.[34] An alternative strategy is to set up an electrochemical cell with the electrodes separated by both a cation-exchange membrane (CEM) as well as an AEM, to block the crossover of anionic proton acceptors and H^+, respectively. The use of two membranes would require CO_2 absorption and release to be time-separated processes occurring after de-acidification and acidification, respectively, as illustrated in Figure S7. This configuration allows the electrochemical cell to be integrated within an aqueous flow battery architecture for simultaneous CCS and energy storage/conversion. A similar concept has recently been demonstrated for electrochemical water desalination by Desai *et al.*[35] Maximizing the overall energy efficiency of the system would require minimizing charge transport losses by using thin membranes with high perm-selectivity, minimizing activation losses by using catalytically active high-surface-area electrodes and redox-active species with fast kinetics, and minimizing mass transport/fluid pumping losses by using carefully engineered electrode pore structures [36, 37] and flow fields.[38-42]

The predicted minimum free energy input for CO_2 separation in this work (16 – 75 kJ/mol$_{CO2}$) appears competitive with other proposed methods (Table 1), particularly those in which alkaline solution is created by splitting or dissociating water. [43-48] As water splitting requires free energy input, theoretical minimum electrical energy inputs for CO_2 separation using these methods range between 119 and 237 kJ/mol$_{CO2}$ (depending on pH at absorption). Because water splitting is also kinetically demanding, requiring catalysts based on Pt and Ru, electrical work requirements for experimentally demonstrated absorptive CO_2 capture using OH^- obtained by reactions following from water splitting are as high as 587 kJ/mol$_{CO2}$..[47] Dissociating H_2O into H^+ and OH^- and using the latter for absorptive CO_2 capture has a lower minimum electrical energy cost, but experimentally demonstrated energy inputs have been fairly high, with 405 [43] and 300 [48] kJ/mol$_{CO2}$ reported in the literature. Much lower energy inputs have been achieved with capture schemes in which redox reactions involving a kinetically accessible substrate, such as a quinone [49] or amine [50], trigger direct binding/release of gaseous CO_2. Indeed, the lowest

experimentally demonstrated electrical work input for an electrochemical CO_2 separation cycle is about 100 kJ/mol$_{CO2,}$ for capturing CO_2 from a flue gas-like (15% CO_2) composition *via* its direct binding to an amine. As the minimum required work input was 15 kJ/mol$_{CO2,}$ this implies a second-law efficiency of 15%. Given that the ideal cycle minimum work input for the electrochemical process considered here for flue gas capture at the lowest outgassing overpressure is about 16 kJ/mol$_{CO2}$, a similar second-law efficiency would yield a similar experimental work input. Recognizing the different values of thermal and electrical work, one could power our process from thermal energy with a heat-to-work efficiency penalty that might vary from ~1/3 for coal combustion to ~60% for a natural gas combined cycle. Assuming the lower value for the efficiency would result in electrochemical CO_2 separation requiring a thermal energy input of around 300 kJ$_{th}$/mol$_{CO2}$ (kJ$_{th}$ denotes thermal energy), which is competitive with more established thermal CO_2 capture methods, particularly those based on concentrated KOH absorption. As discussed above, substantially lower heat inputs may be achieved in practice by operating the cycle with electrochemical acidification/de-acidification in tandem with CO_2 outgassing/invasion.

Table 1. Summary of thermodynamic minimum/ideal cycle and experimentally demonstrated work inputs for CO_2 separation for a variety of electrochemical and thermal methods. Where no method is specified, or the method is not specified in sufficient detail to derive minimum work for an ideal cycle, work input is the thermodynamic minimum given by the exit/inlet pressure ratio, reported in italics. Otherwise, the ideal cycle work/heat input is specified. Experimental work inputs with "th" subscript denote thermal energy inputs, whereas "e" subscript denotes electrical work input.

Method	Exit/inlet Pressure Ratio	Thermodynamic minimum or Ideal Cycle (kJ/mol_{CO2})	Experimental (kJ/mol_{CO2})
	10	*5.6*	
	2500	*19*	
Fuel cell concentrator[47]	2500	119-237[1a]	469-587$_e$[1b]
Salt splitting[43]	N/A[2a]	160[2b]	405$_e$
Direct binding[49]	N/A	17	
Electrochemical amine absorption[50]	6.7	15[4]	100$_e$
Bipolar membrane electrodialysis[48]	2600	20[5a]	150 – 325$_e$[5b]
Quinone PCET[51][6]	--	--	600$_e$
This work	10	16 -75	
	2500	30 -75	
Amine ab-/desorption[52]	8.3	*5.4*[7]	132$_{th}$
Concentrated KOH[8]	375,000	31[8a]	230$_{th}$[8b]

[1a] This technique captures CO_2 into an end state that is not pure gaseous CO_2. As it is based on the operation of an H_2-O_2 fuel cell, the theoretical energy input is that required to split water, which is 119 kJ/mol_{H2O} and thus 119 kJ/mol_{CO2} where CO_2 is captured as HCO_3^-, but 237 kJ/mol_{CO2} where CO_2 is captured as CO_3^{2-}. We do not consider HCO_3^- as a viable end state for capture; however it may be converted to solid carbonates in a process such as the Calera process [53]. [1b]These numbers were added to the value of 350 kJ/mol_{CO2} stated in the publication in order to obtain a fair comparison value of the experimental energetic cost for DAC.

[2a] Exit/inlet pressure ratio is undefined because CO_2 is captured as Na_2CO_3. [2b]Calculated assuming cell operates in steady-state (hydrogen oxidation reaction at pH 0, water reduction at pH 14), and that 100% of H_2 gas generated at the cathode is recovered and fed into the anode.

[4]Calculated for a pressure ratio of 6.7 (15% CO_2 at the inlet, 1 atm CO_2 at the exit), including changes to open-circuit potential from CO_2 binding to amine.

[5a]Calculated for 386 ppm CO_2 at the inlet, 1 atm CO_2 at the exit. [5b]Authors assume from ref. [15] that an additional 200 kJ/mol_{CO2} would be required to operate a spray-based liquid-air contactor, however, we do not consider the contactor work input here.

[6]An inlet composition with 16% CO_2 was reported, but no exit pressure was given. The experimental electrical work input was calculated for a potential of 1.0 V applied across the cell, with CO_2 captured in the form of HCO_3^- and released back to CO_2(g) with 16% mass transport efficiency (see Table 1 in ref. [51]).

[7]Calculated for an inlet and exit compositions of 12% and 100% CO_2, respectively, at a temperature of 35 °C.

[8a]Calculated for 400 ppm CO_2 at the inlet, 150 bar CO_2 at the exit. [8b]Work input excludes electrical work required to operate air-liquid contactor, pellet reactor and auxiliary equipment.

The use of redox-active species and cell architectures that impose minimal kinetic losses while preserving the pH gradient would be crucial to realizing electrochemical CCS at low energetic cost. Watkins *et al.*[51] have demonstrated CO_2 separation from flue gas using a pH gradient created by Pt-catalyzed PCET reactions using benzoquinone and 2,6-dimethylbenzoquinone, however the kinetic sluggishness of the associated redox reactions and the absence of an ion-selective membrane in their design result in a practical work input of 600 kJ/mol_{CO2}. In contrast, we envision the ideal cycle detailed in this work operating with an ion-selective membrane, and able to make use of any redox-active species within a wide array of reactants capable of PCET. In the organic RFB literature, several organic molecules have been shown to have kinetic rate constants on the order of 10^{-3} cm/s or above on inexpensive carbon electrodes[9, 21, 54, 55], demonstrating the wide availability of reactants for CO_2 separation that will impose minimal energetic losses in an electrochemical cell.[54]

In addition to minimal energetic losses, another important criterion for wide scale adoption of CO_2 separation technology is the use of low-cost cell components and working fluids. The process described here can, in principle, use water-soluble molecules and aqueous electrolytes. This is in contrast to most of the electrochemical CO_2 separation methods that do not feature the use of a pH swing which have been described in the literature, involving direct binding of CO_2 to reduced quinones [49, 56] and oxygen-assisted conversion of CO_2 to oxalate species[57] – all of which require more expensive organic solvents to operate. As previously discussed, EMAR has been experimentally demonstrated to require an exceptionally low electrical work input of 100 kJ/mol_{CO2}, which is comparable to what may be expected of our process assuming similar second-law efficiencies.

In this work, we have proposed and performed a thermodynamic analysis of the energetic costs of CO_2 separation from flue gas (0.1 bar CO_2(g)) and air (400 ppm CO_2) using a pH swing created by redox reactions involving PCET. In this scheme, bulk electrolytic reduction results in the formation of alkaline solution, into which CO_2 can be absorbed, whereas oxidation of the resulting solution results in the acidification of the solution, triggering the release of pure CO_2 gas. We examined the effect of buffering from the CO_2-carbonate system on the solution pH during this pH swing, and thus the open-circuit potential of a hypothetical electrochemical cell in a 4-step CO_2

capture-release cycle. The thermodynamic minimum work input varies from 16 to 75 kJ/mol$_{CO2}$ as throughput increases, for both flue gas and DAC, with the potential to go substantially lower if CO_2 capture or release is performed in tandem with electrolytic reduction or oxidation. The lower limit of these values is competitive at a theoretical level with the best electrochemical CO_2 separation method we are aware of, and may result in a practical energetic cost (assuming a heat-to-work conversion efficiency of 1/3) on par with more established absorptive capture methods such as those using concentrated KOH. Additionally, its all-liquid configuration obviates the need for the precipitation and heating of solid carbonates, and compatibility with an aqueous electrolyte and potentially low-cost organic molecules implies that a CCS technology based on this concept has the potential for wide scale practical implementation.

Acknowledgments

This research was supported by a grant from the Harvard University Climate Change Solutions Fund. We thank Daniel Schrag, Daniel Nocera, David Keith, and Andrew Wong for helpful discussions.

References

1. Raupach, M.R., et al., *Global and regional drivers of accelerating CO2 emissions.* Proc Natl Acad Sci U S A, 2007. **104**(24): p. 10288-93.
2. Pacala, S. and R. Socolow, *Stabilization Wedges: Solving the Climate Problem for the Next 50 Years with Current Technologies.* Science, 2004. **305**: p. 968-971.
3. IPCC, *Climate Change 2014: Synthesis Report*, C.W. Team, R.K. Pachauri, and L.A. Meyer, Editors. 2014, IPCC: Geneva, Switzerland.
4. House, K.Z., et al., *The energy penalty of post-combustion CO2 capture & storage and its implications for retrofitting the U.S. installed base.* Energy & Environmental Science, 2009. **2**(2): p. 193.
5. Lackner, K.S., et al., *The urgency of the development of CO2 capture from ambient air.* Proc Natl Acad Sci U S A, 2012. **109**(33): p. 13156-62.
6. House, K.Z., et al., *Economic and energetic analysis of capturing CO2 from ambient air.* Proc Natl Acad Sci U S A, 2011. **108**(51): p. 20428-33.
7. Mahmoudkhani, M. and D.W. Keith, *Low-energy sodium hydroxide recovery for CO2 capture from atmospheric air—Thermodynamic analysis.* International Journal of Greenhouse Gas Control, 2009. **3**(4): p. 376-384.
8. Keith, D.W., et al., *A Process for Capturing CO2 from the Atmosphere.* Joule, 2018.
9. Huskinson, B., Marshak, M. P., Suh, C., Er, S., Gerhardt, M. R., Galvin, C. J., Chen, X., Aspuru-Guzik, A., Gordon, R. G., Aziz, M. J., *A metal-free organic-inorganic aqueous flow battery.* Nature, 2014. **505**(7482): p. 195-8.

10. Costentin, C., *Electrochemical Approach to the Mechanistic Study of Proton-Coupled Electron Transfer.* Chem. Rev., 2008. **108**: p. 2145-2179.
11. Laviron, E., *Electrochemical Reactions with Protonations at Equilibrium Part XII. The $2e^-$, $2H^+$ homogeneous isotopic electron exchange reaction (nine-member square scheme).* Journal of Electroanalytical Chemistry, 1984. **169**: p. 29-46.
12. Quan, M., et al., *Voltammetry of Quinones in Unbuffered Aqueous Solution: Reassessing the Roles of Proton Transfer and Hydrogen Bonding in the Aqueous Electrochemistry of Quinones.* Journal of American Chemical Society, 2007. **129**: p. 12847-12856.
13. Zeebe, R.E. and D. Wolf-Gladrow, *CO2 in Seawater: Equilibrium, Kinetics, Isotopes*. Elsevier Oceanography Series, ed. D. Halpern. Vol. 65. 2005, Amsterdam: Elsevier.
14. Roy, R.N., et al., *The dissociation constants of carbonic acid in seawater at salinities 5 to 45 and temperatures 0 to 45 C.* Marine Chemistry, 1993. **44**: p. 249-267.
15. Stolaroff, J.K., D.W. Keith, and G.V. Lowry, *Carbon Dioxide Capture from Atmospheric Air Using Sodium Hydroxide Spray.* Environ Sci Technol, 2008. **42**: p. 2728-2735.
16. Schulz, K.G., et al., *Determination of the rate constants for the carbon dioxide to bicarbonate inter-conversion in pH-buffered seawater systems.* Marine Chemistry, 2006. **100**(1-2): p. 53-65.
17. da Costa Ores, J., et al., *Purification of carbonic anhydrase from bovine erythrocytes and its application in the enzymic capture of carbon dioxide.* Chemosphere, 2012. **88**(2): p. 255-9.
18. Henderson, M.A., et al., *Target Gas Capture*, U.S.P. Office, Editor. 2014, Carbon Engineering Limited Partnership: United States.
19. Power, I.M., et al., *Carbon sequestration via carbonic anhydrase facilitated magnesium carbonate precipitation.* International Journal of Greenhouse Gas Control, 2013. **16**: p. 145-155.
20. Huynh, M.H.V. and T.J. Meyer, *Proton-Coupled Electron Transfer.* Chemical Reviews, 2007. **107**: p. 5004-5064.
21. Lin, K., et al., *Alkaline quinone flow battery.* Science, 2015. **349**(6255): p. 1529.
22. Lin, K., Gómez-Bombarelli, Rafael, Beh, Eugene S., Tong, Liuchuan, Chen, Qing, Valle, Alvaro, Aspuru-Guzik, Alán, Aziz, Michael J., Gordon, Roy G., *A redox-flow battery with an alloxazine-based organic electrolyte.* Nature Energy, 2016. **1**(9): p. 16102.
23. Yang, B., et al., *High-Performance Aqueous Organic Flow Battery with Quinone-Based Redox Couples at Both Electrodes.* Journal of The Electrochemical Society, 2016. **163**(7): p. A1442-A1449.
24. Kwabi, D.G., et al., *Alkaline quinone flow battery with long lifetime at pH 12.* Joule, 2018. **2**: p. 1907.
25. Hoober-Burkhardt, L., et al., *A new Michael-reaction-resistant benzoquinone for aqueous organic redox flow batteries.* Journal of the Electrochemical Society, 2017. **164**(4): p. A600-A607.
26. Milshtein, J.D., et al., *Voltammetry study of quinoxaline in aqueous electrolytes.* Electrochimica Acta, 2015. **180**: p. 695-704.
27. Jackson, M.N., et al., *Strong Electronic Coupling of Molecular Sites to Graphitic Electrodes via Pyrazine Conjugation.* J Am Chem Soc, 2018. **140**(3): p. 1004-1010.
28. Hollas, A.W., X., Murugesan, V., Nie, Z., Li, B., Reed, D., Liu, J., Sprenkle, V., Wang, W., *A biomimetic high-capacity phenazine-based anolyte for aqueous organic redox flow batteries.* Nature Energy, 2018. **3**(6): p. 508-514.

29. Pratt, H.D., et al., *A polyoxometalate flow battery.* Journal of Power Sources, 2013. **236**: p. 259-264.
30. Chen, J.J., M.D. Symes, and L. Cronin, *Highly reduced and protonated aqueous solutions of [P2W18O62](6-) for on-demand hydrogen generation and energy storage.* Nat Chem, 2018.
31. Rausch, B., et al., *Decoupled catalytic hydrogen evolution from a molecular metal oxide redox mediator in water splitting.* Science, 2014. **345**(6202): p. 1326-1330.
32. Krishnan, C.V., et al., *Electrochemical Measurements of Isopolyoxometalates: 1. pH Dependent Behavior of Sodium Molybdate.* International Journal of Electrochemical Science, 2007. **2**: p. 29-51.
33. Holmes, G. and D.W. Keith, *An air-liquid contactor for large-scale capture of CO2 from air.* Philos Trans A Math Phys Eng Sci, 2012. **370**(1974): p. 4380-403.
34. Varcoe, J.R., et al., *Anion-exchange membranes in electrochemical energy systems.* Energy Environ. Sci., 2014. **7**(10): p. 3135-3191.
35. Desai, D., et al., *Electrochemical Desalination of Seawater and Hypersaline Brines with Coupled Electricity Storage.* ACS Energy Letters, 2018. **3**(2): p. 375-379.
36. Wong, A.A., M.J. Aziz, and S.M. Rubinstein, *Direct visualization of electrochemical reactions and comparison of commercial carbon papers in operando by fluorescence microscopy using a quinone-based flow cell*, in *231st ECS Meeting*. 2017, ECS Transactions: New Orleans, LA.
37. Kok, M.D.R. and J.T. Gostick, *Transport properties of electrospun fibrous membranes with controlled anisotropy.* Journal of Membrane Science, 2015. **473**: p. 237-244.
38. Gerhardt, M.R., A.A. Wong, and M.J. Aziz, *The Effect of Interdigitated Channel and Land Dimensions on Flow Cell Performance.* Journal of the Electrochemical Society, 2018. **165**(11): p. A2625-A2643.
39. Lopes, T., et al., *Assessing the performance of reactant transport layers and flow fields towards oxygen transport: A new imaging method based on chemiluminescence.* Journal of Power Sources, 2015. **274**: p. 382-392.
40. Yin, C., et al., *A coupled three dimensional model of vanadium redox flow battery for flow field designs.* Energy, 2014. **74**: p. 886-895.
41. Ke, X., et al., *Redox flow batteries with serpentine flow fields: Distributions of electrolyte flow reactant penetration into the porous carbon electrodes and effects on performance.* Journal of Power Sources, 2018. **384**: p. 295-302.
42. Messaggi, M., et al., *Analysis of flow field design on vanadium redox flow battery performance: Development of 3D computational fluid dynamic model and experimental validation.* Applied Energy, 2018. **228**: p. 1057-1070.
43. Mehmood, A., et al., *A novel high performance configuration of electrochemical cell to produce alkali for sequestration of carbon dioxide.* Electrochimica Acta, 2016. **219**: p. 655-663.
44. Gilliam, R.J., et al., *Low Voltage Electrochemical Process for Direct Carbon Dioxide Sequestration.* Journal of the Electrochemical Society, 2012. **159**(5): p. B627-B628.
45. Rau, G.H., *Electrochemical CO2 capture and storage with hydrogen generation.* Energy Procedia, 2009. **1**(1): p. 823-828.
46. Datta, S., et al., *Electrochemical CO2 Capture Using Resin-Wafer Electrodeionization.* Industrial & Engineering Chemistry Research, 2013. **52**(43): p. 15177-15186.

47. Eisaman, M., et al. *Energy-efficient electrochemical CO2 capture from the atmosphere*. in *Technical Proceedings of the 2009 Clean Technology Conference and Trade Show*. 2009.
48. Eisaman, M.D., et al., *CO2 separation using bipolar membrane electrodialysis.* Energy Environ. Sci., 2011. **4**(4): p. 1319-1328.
49. Gurkan, B., F. Simeon, and T.A. Hatton, *Quinone Reduction in Ionic Liquids for Electrochemical CO2 Separation.* ACS Sustainable Chemistry & Engineering, 2015. **3**(7): p. 1394-1405.
50. Stern, M.C., et al., *Post-combustion carbon dioxide capture using electrochemically mediated amine regeneration.* Energy & Environmental Science, 2013. **6**(8): p. 2505.
51. Watkins, J.D., et al., *Redox-Mediated Separation of Carbon Dioxide from Flue Gas.* Energy & Fuels, 2015. **29**(11): p. 7508-7515.
52. Goto, K., et al., *Evaluation of Amine-Based Solvent for Post-Combustion Capture of Carbon Dioxide.* Journal of Chemical Engineering of Japan, 2014. **47**(8): p. 663-665.
53. Constanz, B.R., et al., *Methods of Sequestering CO2*, U.S.P. Office, Editor. 2011, Calera Corporation: United States.
54. Chen, Q., M.R. Gerhardt, and M.J. Aziz, *Dissection of the voltage losses of an acidic quinone redox flow battery.* Journal of The Electrochemical Society, 2017. **164**(6): p. A1126-A1132.
55. DeBruler, C., Hu, Bo, Moss, Jared, Luo, Jian, Liu, T. Leo, *A sulfonate-functionalized viologen enabling neutral cation exchange, aqueous organic redox flow batteries toward renewable energy storage.* ACS Energy Lett., 2018. **3**(3): p. 663-668.
56. Scovazzo, P., et al., *Electrochemical Separation and Concentration of <1% Carbon Dioxide from Nitrogen.* Journal of The Electrochemical Society, 2003. **150**(5): p. D91.
57. Al Sadat, W.I. and L. Archer, *The O2-assisted Al/CO2 electrochemical cell: A system for CO2 capture/conversion and electric power generation.* Science Advances, 2016. **2**: p. 1-10.

SUPPORTING INFORMATION

Electrochemical CO_2 Capture Based on Reversible pH Swing

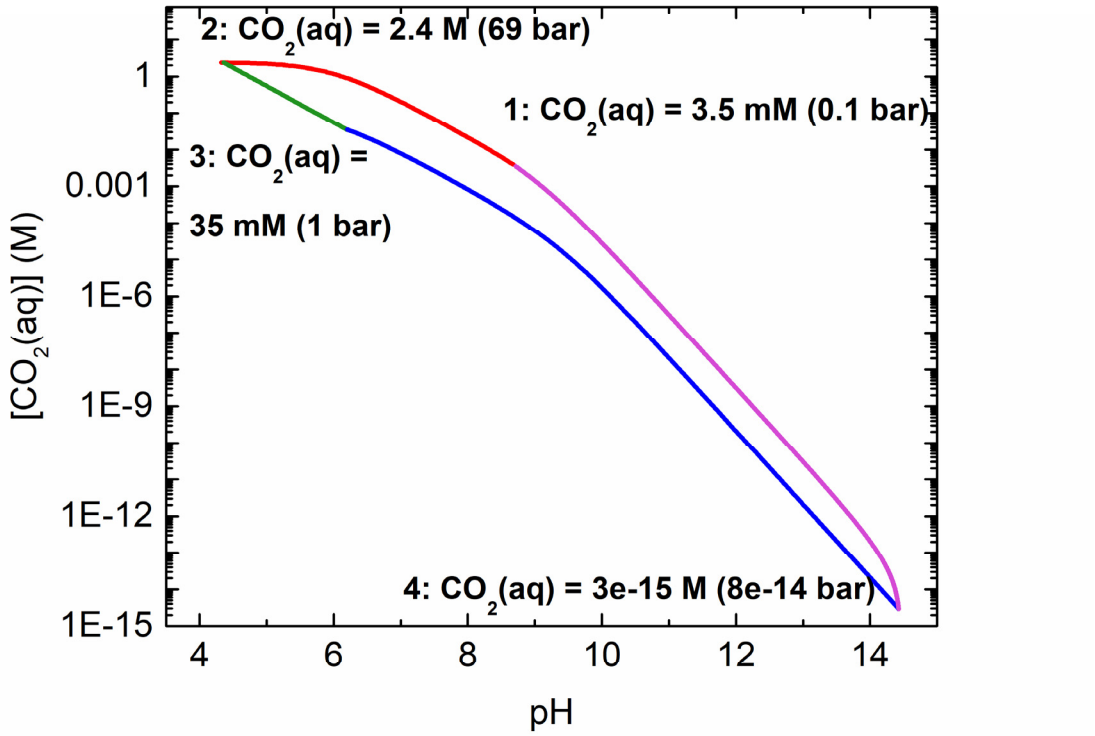

Figure S1. (a) $CO_2(aq)$ vs. pH during the 4-process cycle described in **Figure 4**. Processes 1→2 and 2→3 are depicted with red lines, and processes 3→4 and 4→1 are depicted in blue lines. The equilibrium CO_2 pressure corresponding to each $CO_2(aq)$ is stated.

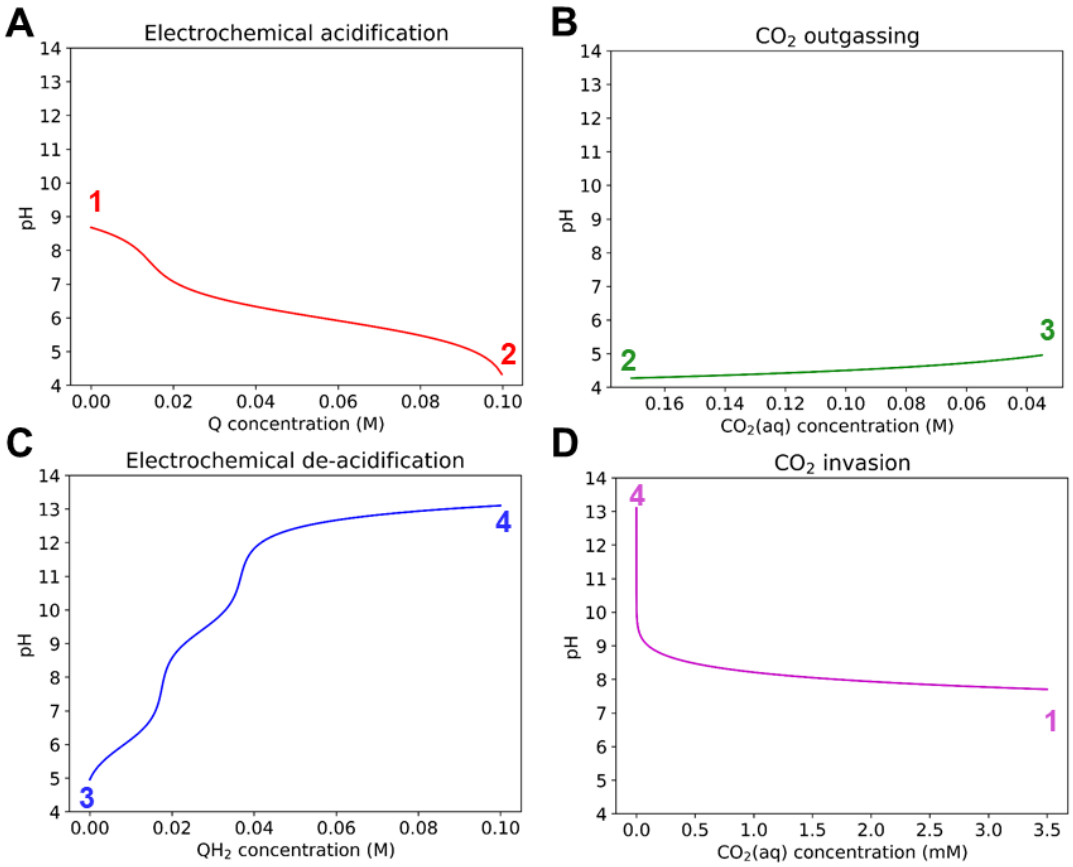

Figure S2. Ideal CO_2 separation cycle for starting *QH_2* concentration of 0.1 M, DIC concentration of 0.175 M and an exit/inlet pressure ratio of 10, which translates to an outgassing overpressure of 5. pH as a function of Q and QH_2 concentration and CO_2(aq) during (a) electrochemical acidification (process 1 → 2) (b) CO_2 outgassing (process 2 → 3) (c) electrochemical de-acidification (process 3 → 4) and (d) CO_2 invasion (process 4 → 1), at the end of which aqueous CO_2 (CO_2(aq)) is assumed to be in equilibrium with 0.1 bar CO_2 gas.

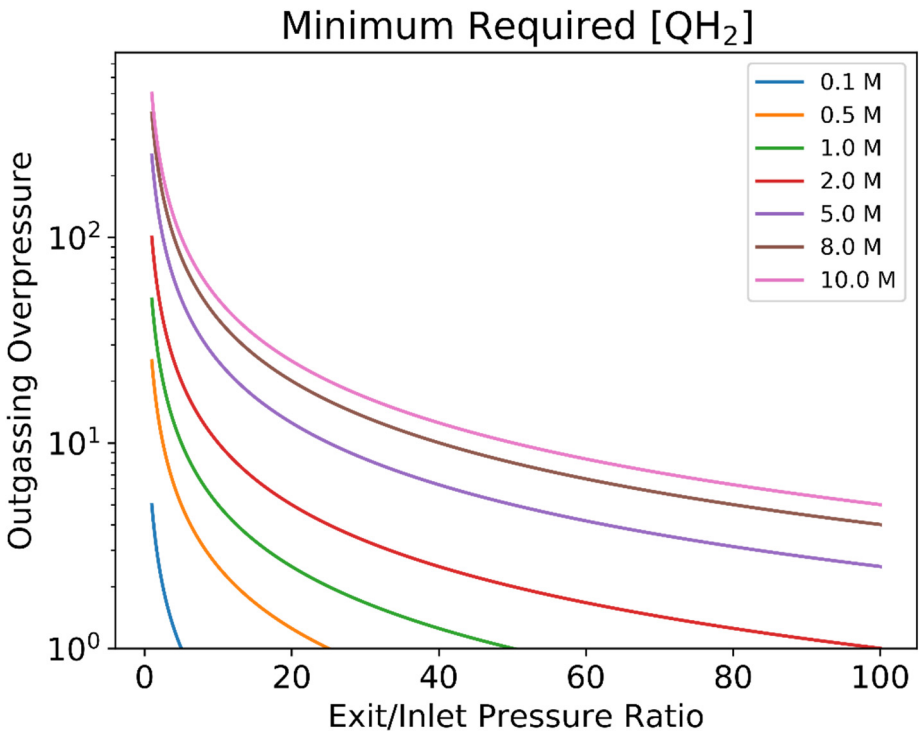

Figure S3. Relationship between outgassing overpressure and exit/inlet pressure ratio for various [QH_2] values at State 1 between 0.1 and 8.0 M, assuming the solution at State 1 is in equilibrium with 0.1 bar CO_2 gas.

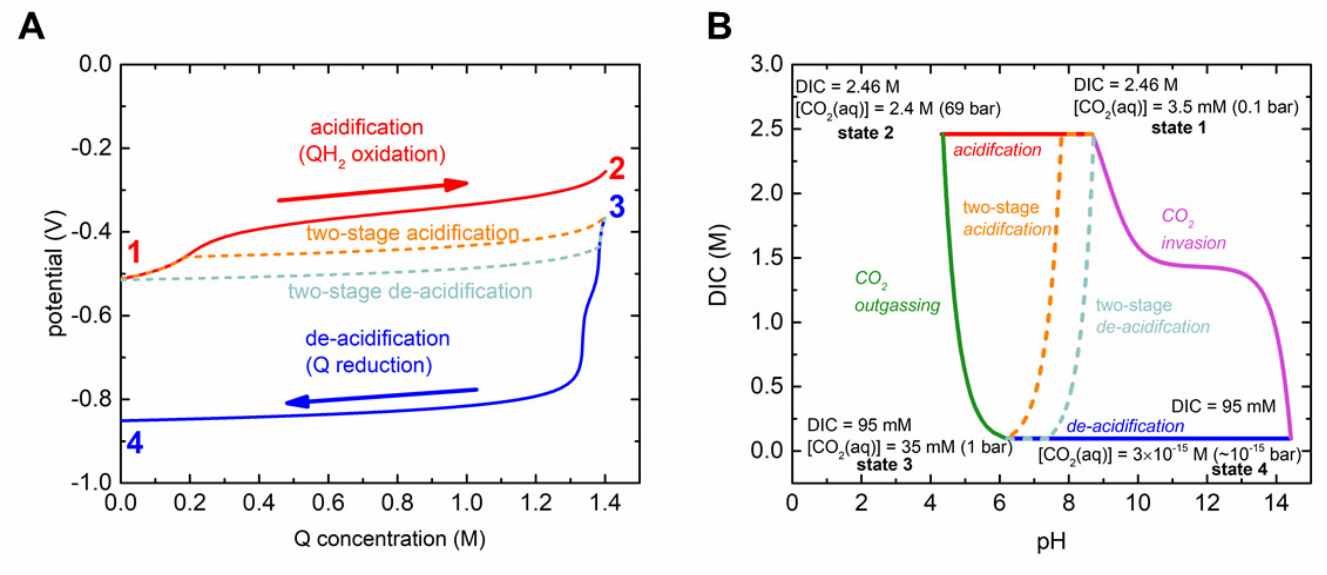

Figure S4. (a) Redox potential *vs* Q concentration and (b) DIC *vs* pH during ideal cycle both without and with two-stage acidification and de-acidification, in which electrochemical acidification/de-acidification is performed in two stages: acidification at constant DIC up to

[CO_2(aq)] = 35 mM, followed by outgassing and further acidification in tandem at constant [CO_2(aq)] until [Q] reaches 1.4 M and de-acidification at constant DIC up to [CO_2(aq)] = 3.5 mM, followed by invasion and further de-acidification in tandem at constant [CO_2(aq)] until [QH_2] reaches 1.4 M.

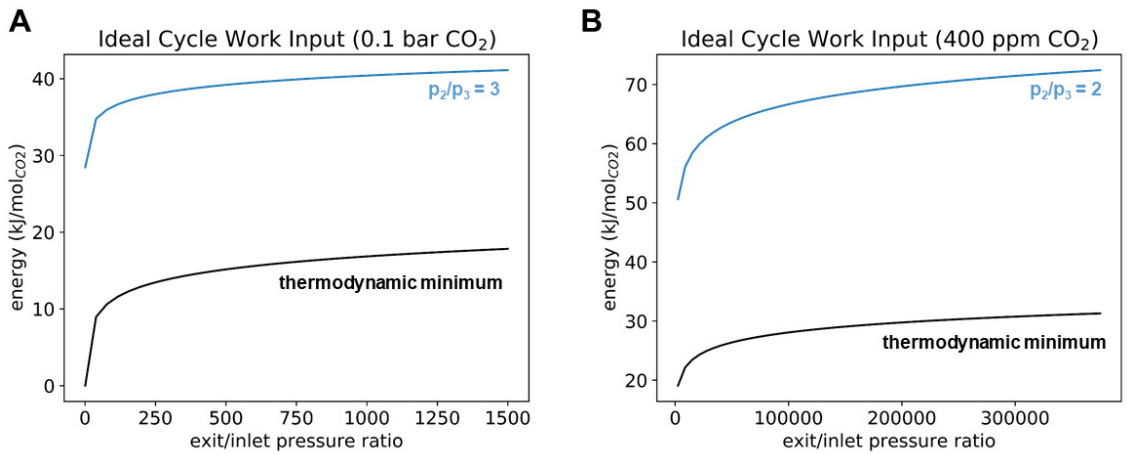

Figure S5. Ideal cycle work vs exit/inlet pressure ratios for inlet streams at (a) 0.1 bar and (b) 400 ppm CO_2. The highest exit/inlet pressure ratio represents an exit pressure of 150 bar CO_2(g), and the maximum overpressure plotted in each case is based on the assumption that QH_2 concentration can reach up to 10 M.

Estimation of final pH after electrochemical de-acidification.

The relative concentration of protonated/deprotonated reduced *Q* is given by the Henderson-Hasselbalch equation, which relates solution pH to the pKa of *QH_2* and the concentrations:

$$pH = pK_a + \log_{10}\frac{[Q^{2-}]}{[QH_2]}. (S1)$$

By assuming that each mole of *QH_2* created by the bulk electrolytic reduction of a mole of *Q* removes 2 moles of H^+ from solution, we can calculate the final pH of a given solution given its initial pH, the concentration of *Q*, and the pK_a of *Q*. The final pH is given by:

$$pH = 14 - pOH, (S2)$$

where *pOH* is defined based on the logarithmic constant for OH^- concentration, as $-\log_{10}[OH^-]$. Because the final pH is the sum of the initial OH^- concentration and OH^- ions created by electrochemical reduction of *Q*, we may re-write the above equation as:

$$pH = 14 + \log_{10}(OH_0^- + OH_n^-), (S3)$$

where OH_0^- is the initial OH^- concentration and OH_n^- represents newly created OH^-. Based on the Henderson-Hasselbalch equation, one can re-express solution pH as a function of starting reactant concentration *Q* and its protonated reduced form, *QH_2*:

$$10^{(pH-\,pK_a)} = \frac{[Q^{2-}]}{[QH_2]} = \frac{[Q-QH_2\,]}{[QH_2]} = \frac{[Q]}{[QH_2]} - 1. (S4)$$

By re-arranging terms and assuming that the formation of each new QH_2 produces two OH^- ions, we obtain an expression for OH_n^-:

$$OH_n^- = \frac{2Q}{1 + 10^{(pH-\,pK_a)}}. (S5)$$

Plugging this expression for OH_n^- into the initial equation provides the full relationship between solution pH, pK_a, initial pH and Q concentration:

$$pH = 14 + \log_{10}\left(10^{(pH_0-14)} + \frac{2Q}{1 + 10^{(pH-\,pK_a)}}\right). (S6)$$

The plot below depicts final pH upon full reduction of Q as a function of pKa for a solution with initial pH 3 and a series of Q concentrations ranging from 50 mM to 2.0 M.

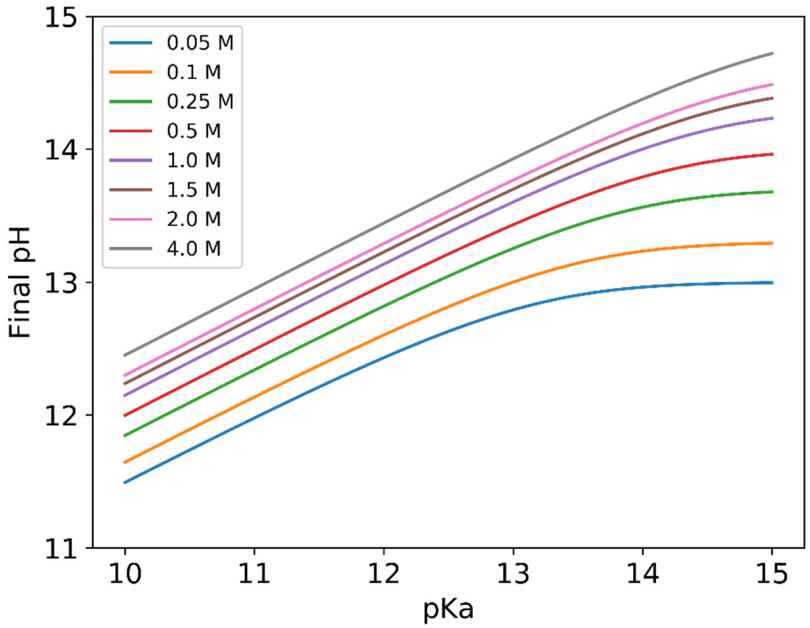

Figure S6. Relationship between pKa of Q and final pH upon reduction of Q based on the solution to implicit equation S6 for a series of Q concentrations between 50 mM and 2.0 M.

It is important to note two assumptions that have been made: (1) the solution is completely unbuffered; and (2) Q has one pKa at which protons are in equilibrium with its deprotonated reduced form. As has been shown in the RFB literature, this is the case for some redox-active species (such as 2,6-dihydroxyanthraquinone [21]) but is not generally true for all reactants capable of PCET, which may have two distinct pKa values for each proton [10]. The main consequence of these assumptions is that the final pH computed above represents an upper limit, as buffering effects will reduce the power of PCET to effect pH shifts, and the presence two distinct pKa values imply a regime in which $2e^-$ reduction will be accompanied by removal of 1 rather than 2 protons from solution.

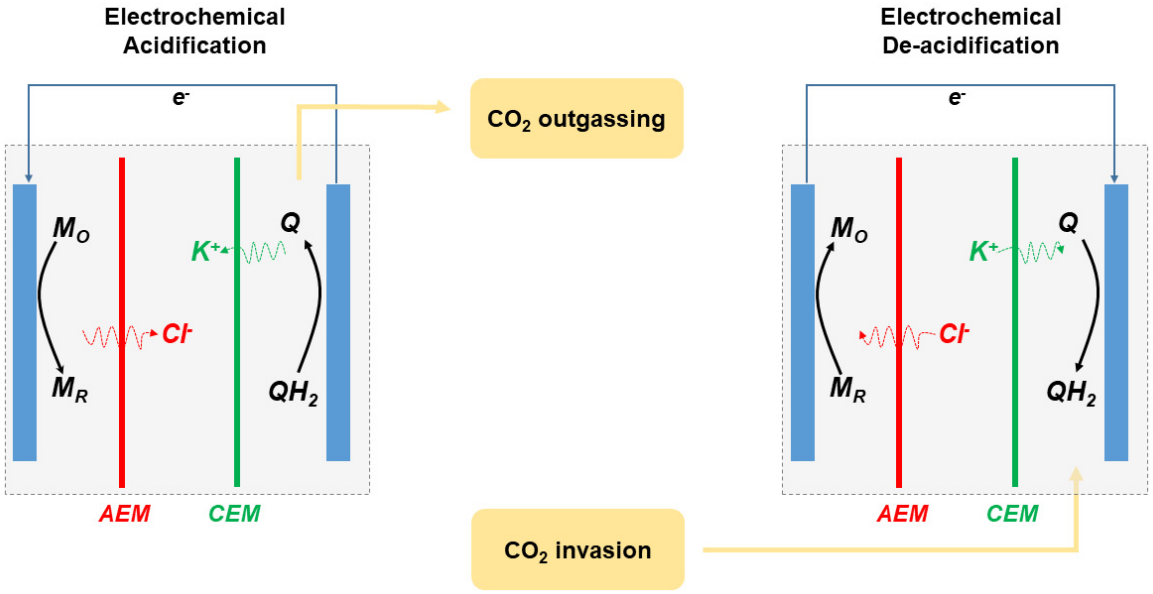

Figure S7. Schematic of two-membrane electrochemical cell, showing how electrochemical acidification and de-acidification processes are integrated with CO_2 outgassing and invasion. A KCl supporting salt is assumed, and K^+ and Cl^- ions move through the CEM and AEM, respectively, to/from a middle electrolyte chamber. M_O and M_R, represent the redox processes occurring counter to Q/QH_2, and could be either symmetric (i.e. QH_2/Q) or asymmetric (i.e. employing some other redox couple), the latter case implying that CCS could be integrated with energy storage.